



SEISMIC PERFORMANCE ASSESSMENT OF L-SHAPED REINFORCED CONCRETE COLUMNS

B. Li⁽¹⁾, T.P. Pham⁽²⁾

⁽¹⁾ Associate Professor in the School of Civil and Environmental Engineering at Nanyang Technological University, Singapore, cbli@ntu.edu.sg

⁽²⁾ Senior Structural Engineer at P&T Consultants, Singapore

Abstract

This paper presents an experimental investigation carried out on ten reinforced concrete (RC) columns with L-shaped sections subjected to simulated seismic loadings. The primary objective of the study was to assess the suitability of using L-shaped RC columns in regions of low-to-moderate seismic risk. The variables of interest included the axial load, loading direction and aspect ratio. The specimen performances were analyzed and discussed in terms of crack patterns, hysteretic response. Results highlighted that the L-shaped columns possess good seismic resistance; Failure mechanism of L-shaped columns was mainly governed by vertical splitting cracks; Shear strength of L-shaped columns were not significantly affected by the level of applied axial force and the direction of horizontal force while initial stiffness was considerably affected by aspect ratio. Further analysis showed that ignoring the contribution of flanges, the shear equation (special provisions for walls) in ACI 318-11 yields good estimations of shear strength for the cases of L-shaped columns.

Keywords: Reinforced Concrete, L-shaped Columns, Shear strength, Seismic

1. Introduction

Irregularly shaped columns are required in some structural designs as at the corner of frame structures or at the enclosure of elevator shafts. Particularly, L-shaped columns are commonly used in existing buildings especially in Singapore; an example is shown in Fig.1.

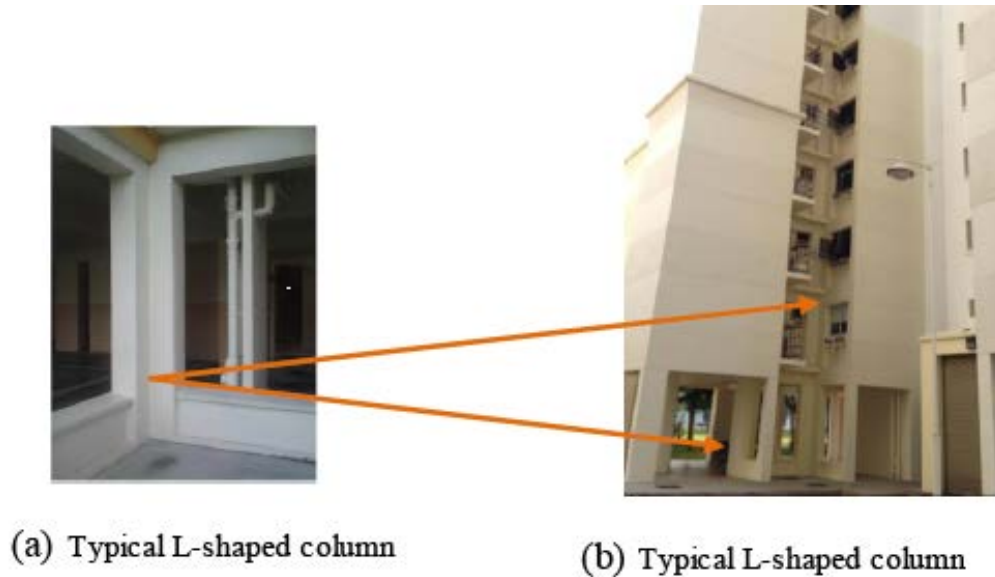


Fig. 1-Typical resident building

Unlike conventional rectangular or circular columns, which have been extensively studied over the years, the load and deformation behavior of L-shaped reinforced concrete columns are rarely available in literature. Marin[1] presented design aids for L-shaped columns using numerical investigations, Ramamurthy and Khan[2] suggested two methods of designs for such columns including the “failure surface” and the “equivalent” rectangular column, while Hsu[3] presented theoretical and experimental investigation for L-shaped columns. Most of the work carried out by the aforementioned researchers focused on static or sectional analysis of such columns. Therefore, the seismic behavior of L-shaped reinforced concrete columns under combined cyclic bending and axial compression is still not well understood. Consequently, in design practice, engineers generally assume that the L-shaped columns respond as two separate perpendicular barbell walls. However, the validity of this assumption has not been well validated. To ascertain the validity of this assumption, seismic responses of the L-shaped columns are studied. The results can also be used to establish the influences of different column sections on the overall performance. This paper aims to provide in-depth understanding of the seismic behavior of existing RC columns with L-shaped section. Ten half-scale RC columns were tested under a combination of a constant axial load and a cyclic loading. The test results were examined in terms of crack patterns, hysteretic response, curvature distribution, displacement decomposition, strain profile and energy dissipation capacity. The results were then compared with predictions based on shear strength from current codes for RC flanged walls.

2. Experimental Program

2.1 Specimen Details

Ten half-scale model columns were designed for the tests with combined axial load and cyclic lateral as shown in Fig. 2 and Table 1. The columns geometries, details and materials were selected to be representative of columns in existing buildings. Column section with equal flange length and the flange length to width ratio in between 2 to 3 are typically found in existing buildings in Singapore. The test columns were divided into two



groups with clear height of 1700 mm or 1200 mm. All specimens had the same cross sectional dimensions of 430x430x170 mm and a longitudinal reinforcement ratio of 2.1% with 12T16 (16 mm). Transverse reinforcement of diameter 6 mm was spaced at 100 mm for columns in Group 1 (1700 mm height) and at 150 mm for columns in Group 2 (1200 mm height). Concrete cover to surface of longitudinal reinforcement was 25mm for all specimens. The longitudinal and transverse reinforcement were characterized by a yield strength of 465 MPa and 467 MPa, respectively. It should be noted that, in many existing buildings, there was no provision available for ductile design therefore transverse reinforcement was detailed typically without C-links as shown in Fig. 2. The shear force V_u corresponding to the development of the theoretical flexural strength of columns were estimated using the material properties obtained through tests and in accordance with the recommendations provided by ACI-318(6). The results are tabulated in Table 1.

Table 1-Summary of test specimens

roup	Specimen	Section $I_w \times I_{wt}$	L (mm)	α°	$\frac{P}{f_c A_g}$	A_s (mm ²)	A_v (MPa)	s (mm)	f_c (MPa)	V_y (kN)	V_u (kN)	I (10 ⁹ mm ⁴)
1	S1	430x430x170	1700	0	0.2	2411.5	56.5	100	29.8	155.9	186.4	1.80
	S2				0.35	2411.5	56.5	100	29.2	199.2	232.7	1.80
	S3			45	0.2	2411.5	56.5	100	29.2	219.7	267.1	2.52
	S4				0.35	2411.5	56.5	100	29.4	261.0	323.7	2.52
	S5			-45	0.2	2411.5	56.5	100	29.1	121.7	181.2	1.09
	S6				0.35	2411.5	56.5	100	29.0	144.0	183.9	1.09
2	S13	430x430x170	1200	0	0.2	2411.5	56.5	150	27.0	216.3	257.3	1.80
	S14				0.35	2411.5	56.5	150	27.4	272.3	316.7	1.80
	S15			45	0.2	2411.5	56.5	150	26.8	300.5	366.7	2.52
	S16				0.35	2411.5	56.5	150	27.2	357.0	436.4	2.52

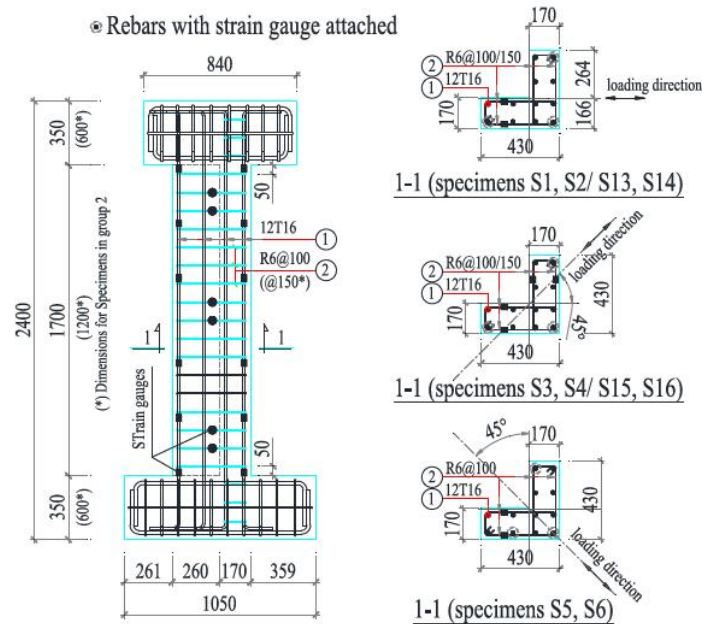


Fig. 2 Detail of specimens

2.2 Test Setup

The test specimens were attached to a loading apparatus as shown in Fig. 3 which enabled the columns to be displaced under double curvature bending. The axial load was slowly applied until the designated level. During each test, the column axial load was maintained by manually adjusting the vertical actuators after each loading step. The lateral load was applied cyclically through the horizontal actuator in a quasi-static fashion as shown in Fig. 3.

3. Experimental Results and Discussions

Results from the tests of ten specimens are presented and discussed in this section. The hysteretic responses of all test specimens are depicted in Fig. 5. The response of test specimens were highlighted by four performance levels: theoretical flexural yielding (PL1), maximum shear force (PL2), shear failure (PL3 - shear strength dropped by 20%) and axial failure (PL4 - when columns were unable to sustain the applied axial force). Generally the hysteretic responses show pinching and reduction of stiffness as well as reduction of shear capacity during repeated cyclic loadings.

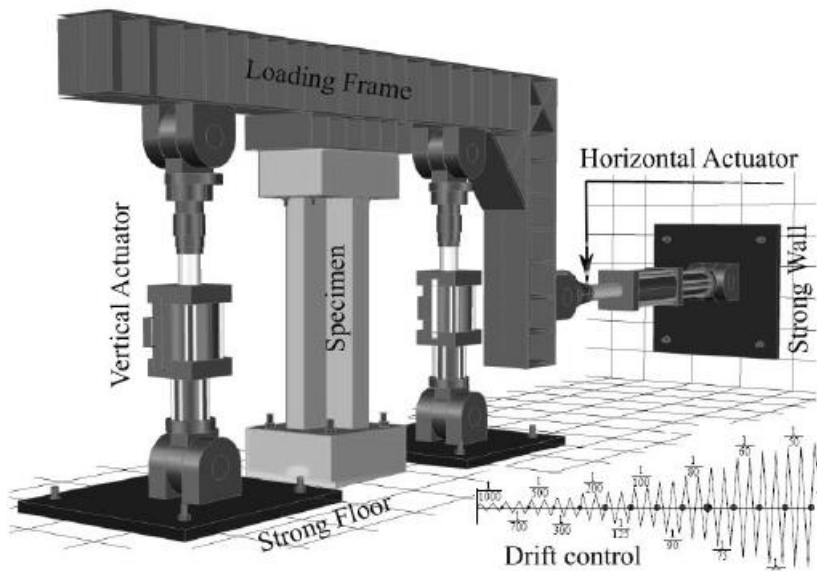


Fig. 3-Experimental setup



Fig. 4- Deformation measurement

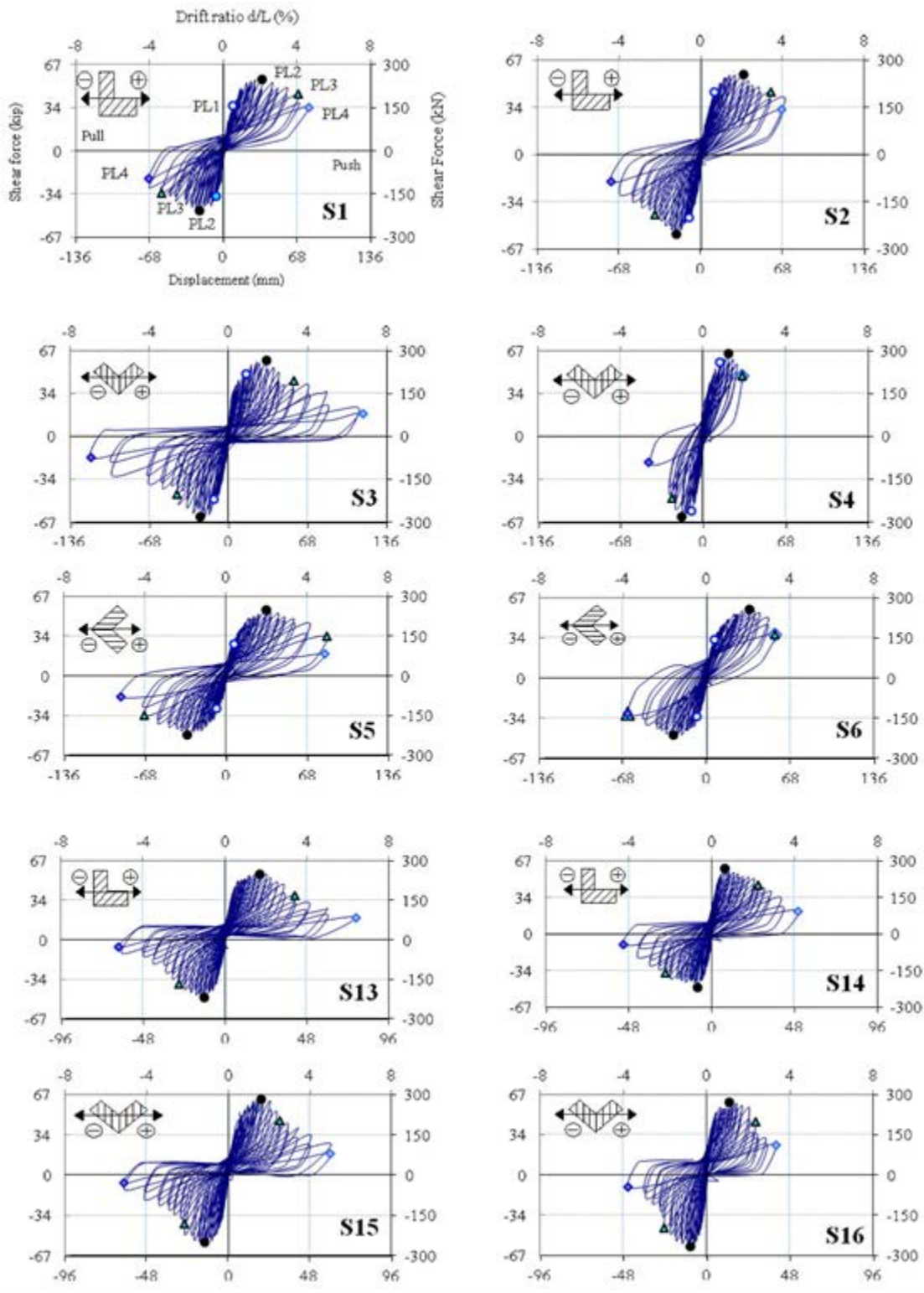


Fig. 5 - Hysteretic response of test specimens

(*PL1*: theoretical flexural yielding, *PL2*: Maximum shear force, *PL3*: Shear failure - shear strength dropped by 20%); *PL4*: Axial failure - when columns were unable to sustain the applied axial force)

All six specimens in Group 1 experienced yielding of longitudinal reinforcement before attaining maximum shear force while none of the specimens in Group 2 developed flexural yielding. Details of cracking patterns, failure mode, hysteretic response (including yield displacement, initial stiffness, shear strength, drift capacity) curvature distribution, displacement decomposition and energy dissipation capacity are as follows:

3.1 Cracking patterns and failure modes

Cracks on all surfaces of the specimens were marked at every peak displacement stage. Cracking patterns at maximum shear force and at axial failure are shown in Figs. 6, 7. From the observed cracking patterns, two failure modes were identified.

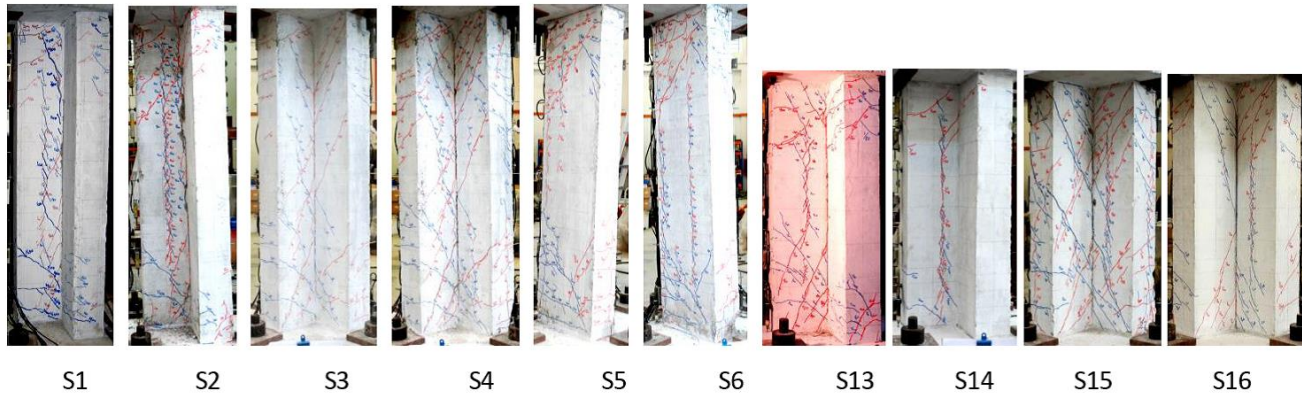


Fig. 5-Crack patterns at maximum shear force of test specimens

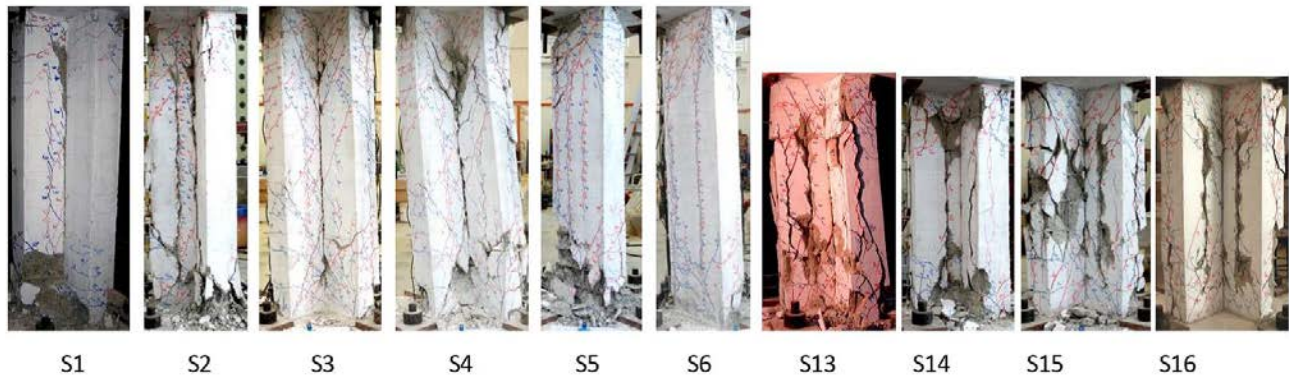


Fig. 6-Axial failure of test specimens

The first failure mode occurred in Specimens S1, S2, S3, S4, S13, S14, S15 and S16 due to the development of vertical splitting cracks along longitudinal reinforcements. The typical illustration is shown in Fig. 8. In these specimens, flexural cracks perpendicular to column axis developed first in the regions close to the top and bottom ends when loaded to a drift ratio of 0.33%, 0.2% for columns under principal loading direction and diagonal direction, respectively regardless of aspect ratio. When increasing drift ratio by 0.1%, the flexural cracks in horizontal direction gradually changed to diagonal direction and extended to the column web due to the appearance of high shear stress. It was also observed that in columns with higher axial load, both the flexural and diagonal cracks decreased in size and length. The diagonal cracks initially formed at an angle of around 45° to the column vertical axis, and increased with the applied shear force, eventually reaching a maximum angle of 60°. Extensive diagonal cracks formed in the specimens tested in strongest direction (Specimens S3, S4, S15 and S16). However, these diagonal cracks did not directly lead to the failure of the specimens, rather, the failure of these specimens can be mainly attributed by the vertical cracks along center longitudinal bars. These cracks

occurred earlier in Specimens with higher axial force and were observed first at a drift ratio of 0.8% in S1 and S13, 0.67% in Specimens S2 and S14, S15 and 0.5% in specimens S3, S4 and S16. At the end of the tests, concrete crushing occurred at both ends of test specimens and on the surface of vertical splitting cracks (see Fig. 7). Concrete spalling was also observed along the height of specimens. The failure mechanism depicted in Fig. 7 was similar to the failure pattern in the tests of square and rectangular RC columns observed previously by the authors.[7] This unique failure mechanism has also been explained by the authors in another work.[8] In that work, Pham and Li[8] proposed a failure mechanism for the splitting failure as shown in Fig. 9. According to the proposed mechanism, the applied axial force (P), applied bending moment (M) and applied shear force (V) are carried out by a summation of internal forces: Compression force ($C1$ and $C2$) acting in both column ends; Diagonal sliding shear stress ($S1$ and $S2$) of concrete in compression zones; Vertical sliding shear stress ($S3$) in concrete along potential splitting plane and tensile stress in transverse reinforcement (T_s). By using the test results, Pham and Li [8] proved that the splitting failure occurs when the vertical sliding shear stress ($S3$) reaches its ultimate sliding shear strength. The analytical results matched reasonably with the test observation and shear strength of the test columns.

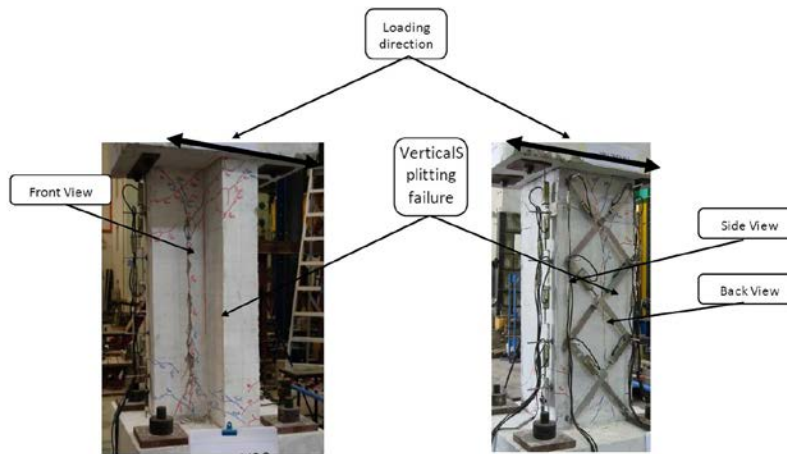


Fig. 7-Typical failure mode

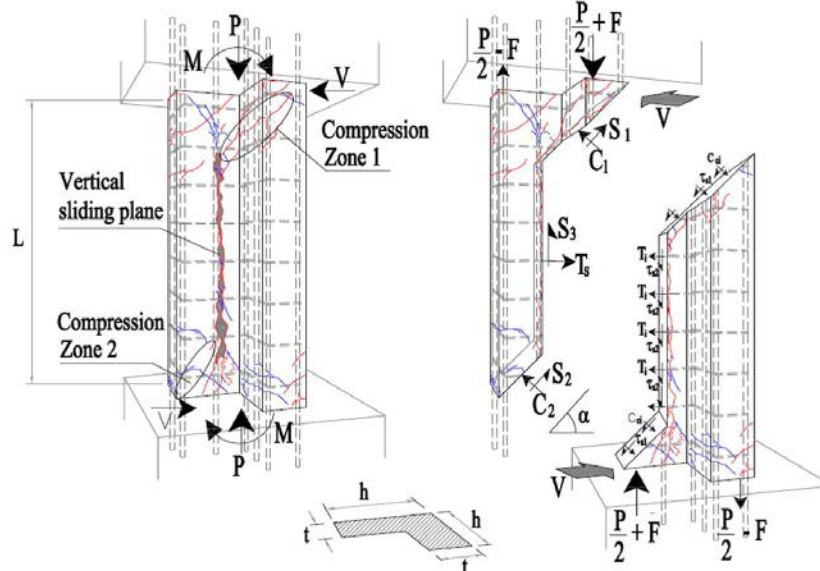


Fig. 8-Failure mechanism

The second failure mode was observed in specimens tested in weakest loading direction, S5 and S6 those failed due to the development of plastic hinges forming at both columns ends and leading to crushing of concrete as



well as buckling of longitudinal reinforcement. In these two specimens flexural cracks developed at column ends from a drift ratio of 0.2% and 0.33% in S5 and S6, respectively. No sign of shear cracks was observed up to a drift ratio 1% in S5 and 0.8% in S6. Vertical cracks were also observed along the center bars of both flanges in loading to a drift of 1.67% in S5 and 1.43% in S6 however these cracks did not propagate and had a negligible contribution to the failure.

3.2 Hysteretic response

Hysteretic response of test specimens (Fig. 5) was assessed by analyzing yield displacement, initial stiffness, maximum shear force and drift capacity.

3.3 Shear Strength

Shear strength was normalized by dividing the attained maximum shear force (from hysteretic response) to the cross sectional area of specimen and square root of compressive concrete strength (V_{max}/A_g). The results in Fig. 10 show that the normalized shear strength of all test specimens was varied within a short range from 0.36 to 0.44. The maximum shear force of L-shaped columns was not significantly affected by applied axial force levels. For the first group, when the axial force ratio increased by 75% from 0.2 to 0.35 the shear strength was increased only by 11%, 4% and 0.1% for columns in directions 0° , 45° and -45° , respectively. The increments were also around 3.9% and 1.9% for the group of short columns. This observation can be explained by the high value of the depth-to-width ratio in L-shaped column sections in which the mechanism of axial force influencing the shear strength through compression diagonal strut might not mobilize.

Another observation showed that, although the section is not symmetrical, the shear strength was surprisingly not remarkably affected by the loading direction. Highest change in shear strength of 19.8% was found in a specimen of the first group when tested under the applied axial ratio of 0.2 and the loading direction was changed from 0° to 45° (S1 versus S3). The changes in short columns were 10.3% and 13.5% for the columns tested under axial load of 0.2 and 0.35, respectively. Nonetheless loading direction seems to be sensitive to the shear strength rather than the applied axial force.

3.4 Drift capacities

Drift capacities, drift ratios recorded at each the performance level (as defined previously), are shown in the hysteretic responses of each specimen in Fig. 5. The effects of the test parameters on the drift capacities of L-shaped columns are depicted in Fig. 10. The results show that drift ratios at PL2, PL3 and PL4 of all specimens reduced with an increase of axial force or the change of loading direction from weaker direction to stronger direction. With an increment in the initial stiffness, the specimen behave in a more brittle manner which resulting in a lower drift capacity. The results also show that when the axial force ratio increased from 0.2 to 0.35, the most significant change in drift capacity was observed in specimen with clear height of 1.7m and tested in the strongest loading directions. From S3 to S4 the drift ratio was reduced by 24.4%, 75% and 82.2% for the points at maximum shear force, shear failure and axial failure, respectively. With respect to the effect of loading direction, the change in drift capacities was most notably observed in S2 and S4 which tested under the same axial force ratio of 0.35. The change in loading direction by 45° from S2 to S4 resulted in the reductions in drift capacities of 25%, 68% and 85% for the performance levels PL2, PL3 and PL4, respectively.

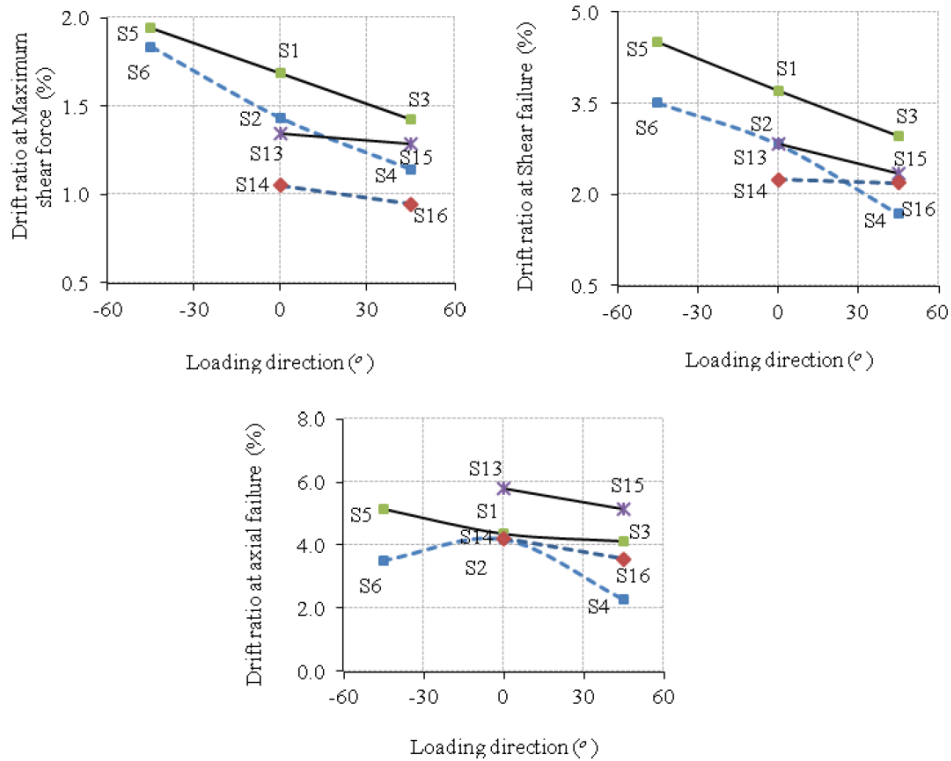


Fig. 10-Effects of test parameters on drift capacity

4. Shear Strength Evaluation

The effect of flanges on the shear strength of L-shaped RC columns has not been well studied and is usually ignored in design practice which is similar to the observations in RC flanged walls. In this section, shear strength models, which were originally proposed for walls, will be assessed and compared with the test results of L-shaped columns to evaluate the possibility in the application of these models for L-shaped columns.

Three equations based on the procedures provided in Chapter 21 of ACI 318-11[6] Chapter 11 of ACI 318-11, and ASCE 43[10] are used herein to predict the peak shear resistance of the test L-shaped columns. ACI 318-11 provides two semi-empirical equations, both based on the modified truss analogy approach, to evaluate the strength of squat reinforced concrete walls. The equation in Section 21.9 of ACI 318-11 (Special reinforced concrete structural walls and coupling beams) is intended for seismic design. The equation in Section 11.9 (Special provisions for walls), is to be used for general design.

Below Equation is from Section 21.9 of ACI 318-11, thereafter namely Equation 1:

$$V_1 = (\alpha_c \sqrt{f'_c} + \rho_t f_{yt}) 0.8 A_w \leq 0.83 \sqrt{f'_c} A_w \quad (4)$$

where the coefficient α_c is 3.0 for $h_w / l_w \leq 1.5$, is 2.0 for $h_w / l_w \geq 2.0$, and varies linearly between 3.0 and 2.0 for h_w / l_w between 1.5 and 2.0.

The procedure for evaluating the shear strength per Section 11.9 of ACI 318-11, thereafter namely Equation 2, is given by the following four equations.

$$V_2 = V_c + V_s \leq 0.83 \sqrt{f'_c} t_w d \quad (5)$$



$$V_c = 0.274\sqrt{f'_c}t_w d_1 + \frac{P_u d}{4l_w} \quad (6)$$

$$V_c = \left[0.05\sqrt{f'_c} + l_w \left(0.104\sqrt{f'_c} + \frac{0.2P_u}{l_w t_w} \right) / \left(\frac{M_u}{V_u} - \frac{l_w}{2} \right) \right] t_w d \quad (7)$$

$$V_s = \frac{A_v f_{yt} d}{s} \quad (8)$$

The following conditions apply per Section 11.9.6 of ACI 318-11: the shear strength provided by concrete is taken as the lesser of the values provided by equations (6) and (7); and equation (7) does not apply when $M_u/V_u - l_w/2 \leq 0$. ACI 318-11 Chapter 11 imposes an upper limit of 0.83 MPa (10 psi) on the ultimate shear stress. The ratio of the minimum horizontal reinforcement is restricted to 0.25%; the ratio of minimum vertical reinforcement ratio is determined by

$$\rho_v = 0.0025 + 0.5 \left(2.5 - \frac{h_w}{l_w} \right) (\rho_t - 0.0025) \quad (9)$$

The Equation described by Eq. 4-3 and 4-4 in ASCE 43-05 [3] to compute the shear strength of squat walls with barbells or flanges, thereafter namely Equation 3. The Equation is applicable for walls with the aspect ratios h_w/l_w of 2 or less and vertical and horizontal reinforcement ratios less than or equal to 1%. If the reinforcement ratios exceed 1%, the combined reinforcement ratio ρ_{se} , (calculated using Eq.12) is limited to 1%. ASCE 43 imposes an upper limit of $1.66\sqrt{f'_c}$ MPa (20 psi) on the ultimate shear stress.

$$V_3 = v_n d t_w \quad (10)$$

$$v_n = 0.689\sqrt{f'_c} - 0.282\sqrt{f'_c} \left(\frac{h_w}{l_w} - 0.5 \right) + \frac{P}{4l_w t_w} + \rho_{se} f_y \leq 1.66\sqrt{f'_c} \quad (11)$$

$$\rho_{se} = A\rho_v + B\rho_t \quad (12)$$

The shear strength prediction results for L-shaped columns tested in principal direction are shown in Table 5

Table 2. Estimation of shear strength for L-shaped columns

Specimen	V_{test} (kN)	Prediction (kN)					
		V_1	V_1/V_{test}	V_2	V_2/V_{test}	V_3	V_3/V_{test}
S1	228.6	326.7	1.43	215.0	0.94	370.0	1.62
S2	254.2	326.7	1.29	262.9	1.03	392.1	1.54
S13	234.4	315.3	1.35	234.1	1.00	378.3	1.61
S14	244.7	315.3	1.29	318.8	1.30	378.3	1.55
S7	142.2	235.8	1.66	156.1	1.10	282.9	1.99
S8	161.2	237.3	1.47	135.2	0.84	284.8	1.77
Mean			1.41		1.04		1.68
CoV			0.106		0.148		0.109



5. Summary and Conclusions

An experimental program was carried out on ten reinforced concrete columns with L-shaped sections under simulated gravity and seismic loads. The obtained results were analyzed, discussed and evaluated by the current assessment code for RC walls. The following conclusions are drawn:

1. Two failure modes were observed whereas eight out of ten specimens failed by the development of the vertical splitting cracks along the longitudinal reinforcement prior to reaching shear strength. These cracks separated the columns vertically, causing crushing and spalling of concrete in the sliding surface. The second failure mode was caused by the development of plastic hinges which lead to the crushing of concrete and the buckling of reinforcing bars at columns ends. This failure was observed in two specimens tested under weakest loading direction. There was no significant difference in the hysteretic response between the two failure modes.
2. Previous studies have found that axial compressive force does not significantly affect the nominal yield curvature. However, this finding was only validated for walls with axial force ratio less than 0.1. For L-shaped columns with an axial force ratio of 0.2 to 0.35, yield curvature varies inversely with applied axial force and also affected by the loading direction.
3. The shear strength model provided in section 11.9 in ACI 318-11 for RC flanged walls yields a good prediction for shear strength of L-shaped columns by ignoring the contribution of flanges. The estimated results match well with the shear strength of L-shaped columns tested in principal direction.

5. References

- [1] Marin, J (1979): Design aids for L-shaped reinforced concrete columns. *American Concrete Institute*, **76**, 1197-1216.
- [2] Ramamurthy, L. N. and Hafeez Khan, T. A (1983): L-shaped column design for biaxial eccentricity, *Structural Engineering*, **109**(8), 1903-1917.
- [3] Hsu, C.-T. T (1985): Biaxial loaded L-shaped reinforced concrete columns, *structural engineering*, **111**(12), 2576-2595.
- [4] Tran, C. T. N. and Li, B (2012): Initial Stiffness of Reinforced Concrete Columns with Moderate Aspect Ratios, *Advances in Structural Engineering*, **15**(2), 265-276.
- [5] Pham, T. P. and Li, B (2013): Seismic Behavior of RC Columns under Different Loading Directions, *ACI Structural Journal*, **110**(5), 833-843.
- [6] ACI Committee 318(2008): Building Code Requirements for Structural Concrete (ACI 318-11) and Commentary, *American Concrete Institute*, Farmington Hills, MI.
- [7] Pham, T. P. and Li, B. (2014): Seismic performance of RC Columns with plain longitudinal bars, *ACI Structural Journal*, **111**(6).
- [8] Pham, T. P. and Li, B (2013): Splitting Failure of Reinforced Concrete Columns, *Journal of Structural Engineering*, 10.
- [9] Priestley, M. J. N. and Kowalsky, M. J (1998): Aspects of drift and ductility capacity of rectangular cantilever structural walls, *Bulletin of the New Zealand National Society for Earthquake Engineering*, **31**(2), 73-85.
- [10] ASCE/SEI 43-05 (2005): Seismic design criteria for structures, systems, and components in nuclear facilities, *ASCE Standard*.